Proceedings of ASME Turbo Expo 2014: Turbine Technical Conference and Exposition
GT2014
June 16 – 20, 2014, Düsseldorf, Germany

GT2014-26311

STUDY OF UNSTEADY HEAT TRANSFER AS A KEY PARAMETER TO CHARACTERIZE LIMIT CYCLE OF HIGH AMPLITUDE PRESSURE OSCILLATIONS

Mina Shahi* **Jim.B.W.Kok** **J.C. Roman Casado**

Artur.K.Pozarlik

University of Twente, Faculty of Engineering Technology, Laboratory of Thermal Engineering
Enschede, The Netherlands
*Email: m.shahi@utwente.nl

ABSTRACT

The objective of the studies presented in this paper is the numerical prediction of unsteady heat flux and pressure fluctuations during the unstable regime of a combustor. The studied laboratory-scale lean partially premixed combustor was built in the LIMOUSINE project, to explore the mechanisms driving thermo-acoustic instabilities in conditions representative of gas turbine combustors.
Due to the thermal interaction between hot gases and the colder liner wall, and also the correlation between gas temperature , density and speed of sound, prediction of the transient heat transfer rate is of high importance. In this paper analysis of transient heat transfer is conducted by coupling of fluid flow and solid body (liner) in one computational domain and thereby taking into account the thermal convection with the environment around the combustor and also the heat conduction transients within the liner. Conjugate heat transfer modeling can give access to the transient temperature distribution in the structure of the combustor which is important for the dynamic heat storage. Also this can be used to estimate the thermal stresses and creep strain as required to evaluate the lifetime assessment of the combustor. In this work the commercial CFD code ANSYS CFX is used to solve the problem, in which fluid and solid regions are solved simultaneously with a finite volume approach. In the fluid region, three dimensional compressible Reynolds Averaged Navier-Stokes equations are solved, while for the solid region only the enthalpy conservation equation is solved. To remove any interpolation errors, in all cases the skin (interface) mesh cells for both the fluid and solid are similar in resolution on either side of the interface. By comparing heat release and pressure data available from the measurements it follows that this simulation can give more accurate prediction of the amplitudes of thermoacoustic instabilities as compared to the solution with imposed thermal boundary conditions (such as isothermal). In the latter case the time history of heat accumulation in the solid is predicted incorrectly. Because the spatial scales of the solid temperature profiles are different in case of steady state or transient oscillatory heat transfer, care has to be taken in the meshing in these two situations. When meshing for a transient oscillatory heat transfer case, the solid mesh resolution needs to be adapted to the thermal penetration depth of the surface temperature oscillations. Hence for the transient heat transfer in limit cycle combustion oscillations, the meshing strategy and size of the grid in the solid part of the domain will play a very important role in determining the magnitude for the pressure fluctuations.

KEYWORDS: *Combustion modeling, Conjugate heat transfer, RANS solver, Partially premixed combustion, penetration depth*

NOMENCLATURE.

SYMBOLS

f	Frequency
h	Heat transfer coefficient
h_s	Solid enthalpy
P	Pressure
T	Temperature
ρ	Fluid density
ρ_s	Solid density
λ	Air excess ratio
λ_s	Solid heat conductivity
u	Velocity
α	thermal diffusivity

ACRONYMS

BVM	Burning Velocity Model
CHT	Conjugate Heat Transfer
FFT	Fast Fourier Transform
HTC	Heat Transfer Coefficient
LCO	Limit Cycle Oscillations
LES	Large Eddy Simulation
RANS	Reynolds Average Navier-Stokes
SST	Shear Stress Transport Turbulence

INTRODUCTION.

An accurate prediction of the heat transfer across the walls of a combustion chamber in a gas turbine is of high importance especially when the inlet temperature of the turbine increases. Researches in this topic are mainly related to the heat transfer of gas turbine blades, to calculate the heat transfer around the bucket and nozzles by conducting either steady state or transient Conjugated Heat Transfer calculations (CHT) [1-5]. In these researches separate solvers and codes have been used to solve the transport equations in the fluid and solid domains. Therefore the accuracy of results relies heavily on the coupling and interface data exchange between the flow solver and the solid heat conduction code.

The aim of this paper is to investigate transient heat transfer to the liner in the situation of limit cycle flow variations and the resulting effects on acoustics of the system due to variable heat flux on the wall. In addition these data could be used for a fatigue failure analysis. In earlier work of Shahi et al. [6] the effect of cooling on the wall has been taken into account by specifying a wall heat flux correlation as a modified thermal wall boundary condition. A Heat Transfer Coefficient (HTC) model was used and a 1-D heat transfer through the wall was assumed, rather than the adiabatic or isothermal assumption. Since the largest temperature gradients will be across the liner, not along it, 1D heat transfer across the liner should be a good modeling approximation. However by applying the HTC model as the liner boundary condition in a fluid-domain-only calculation, the wall heat transfer is instantaneous, without any delay due to the wall thermal inertia. In case of a limit cycle oscillation of the combustion process, with accompanying gas temperature fluctuations, at a frequency of order of magnitude 300 Hz, the neglect of the wall thermal inertia will not be correct any more. The hot gas temperature fluctuations will have a limited depth of penetration into the liner wall, and the time averaged wall temperature profile may be different from the profile predicted by the HTC model. Hence the time mean heat exchange and gas temperature can be changed due to the dynamics of the heat transfer and wall heat storage. Beside that in order to access to the life assessment of the structure, it is necessary to evaluate the temperature distribution and its oscillation amplitudes within and along the liner of the combustion chamber especially in the case that limit cycle combustion oscillations occur.

In this work the liquid and solid computational domains are solved simultaneously in a monolithic approach, giving more accurate prediction of the transient heat transfer from/to the liner. This approach removes the uncertainties related to the coupling strategy as is necessary in partitioned approaches.

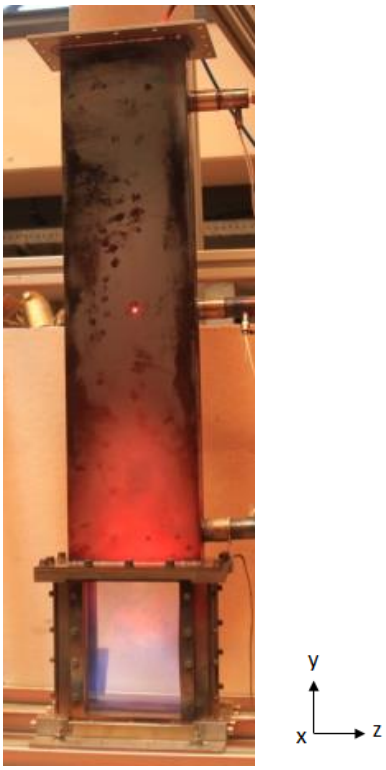

FIGURE 1: THE LIMOUSINE COMBUSTOR: THERMAL LOAD ON THE STRUCTURE IN AN UNSTABLE OPERATING CONDITION. RED DOT ON STRUCTURE CENTER IS THE LASER VIBROMETER BEAM

High mechanical vibration amplitudes of the combustion liners at high temperature driven by thermoacoustic instabilities will lead to high-cycle fatigue damage. The effects of the enhanced heat transfer during the limit cycle result in a damage on the top liner (E.g. the hot section of a typical can type combustor) where there is interaction between the flame and the wall.

In view of the above, a transient flame -wall interaction analysis was performed by means of the Conjugated Heat Transfer model. This was validated by means of the results of the experiments considering the transient pressure inside the combustor as a validating tool. The presented method for, and predicted results of, the temperature distribution by means of conjugated model can be used for the creep analysis of the liner of the combustor.

In the first part, this paper presents the computational domain and grid resolution focused mainly on the solid region. Then the used numerical approaches are described, and finally the results of the simulations are presented and discussed.

Simulation results show the effectiveness of the approaches and solid grid size on the characteristics of limit cycle of pressure oscillations.

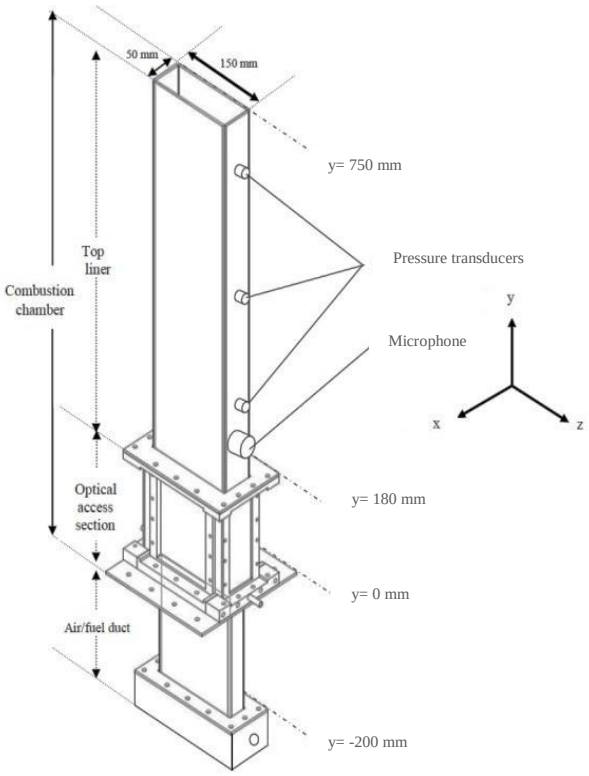

(a)

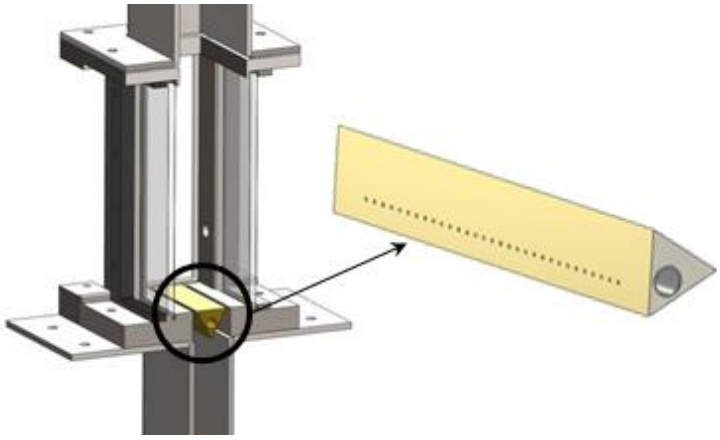

(b)

FIGURE 2: (A) GENERAL VIEW OF THE SET UP (B) CLOSE UP VIEW OF THE WEDGE AND INJECTION HOLES

COMPUTATIONAL DOMAIN AND GRIDS.

The LIMOUSINE burner configuration is displayed in limit cycle oscillatory operation in figure 1. Clearly the high wall temperature zone can be observed where the flame is located. A sketch of the combustor lay out with sensor locations is given in figure 2. This combustor is different from the industrial gas turbine combustors, as it has an open outlet, imposing atmospheric mean pressure in the combustor. But it does share with gas turbine burners a flame stabilized by a recirculation area, a narrow burner flow passage, an upstream cold flow area and an acoustically closed air inlet. Therefore it is expected that the limit cycle phenomenon under study is essentially identical, and the generated data can be used in the subsequent investigation of flame characteristics.

The computational domain examined in this work, including both solid and fluid regions is sketched in figure 3. The schematic of this coupled system is also shown in figure 4. The simulation takes the advantage of the prismatic geometry, by considering only a thin slice of the combustor. Therefore the span wise size of the numerical domain is 4 mm wide with symmetry enforced on each side.

The computational domain is composed of the fluid region and the solid region surrounding the fluid. A structured mesh system is employed for discretization of the governing equations. The impact of the meshing technology and sensitivity of the results on the grid have been studied by authors in [7] focusing on the fluid-only simulation. All the meshes used in this study are generated using the meshing tool ANSYS Workbench 14.5. Detail properties of the grid in the fluid region are presented in table 1. For the sake of reducing the necessary computational efforts the solid domain has been simplified. Therefore it has been modeled without considering quartz glass windows or ports for thermocouples and pressure transducers. The solid mesh has been created in a way that the fluid and solid grids are conformal in the interface. The solid mesh requirements are less stringent, as the volume of the solid structure is very small as compared to the fluid zone, allowing a fine mesh without large numbers of mesh points. In this work three different grids have been generated as presented in table 2. In the third mesh (M3) the inflated layer option in the x-direction has been used, with a mesh spacing which is gradually growing towards the center of the liner. This spatial refinement from the initial coarse mesh (M1) to the final version (M3) has been done based on the temperature distribution in the thermal penetration depth to ensure the obtained results are grid independent (See figure 5 and Annex A). The dependency of predicted results on the solid grid will be discussed in the result section. Physical properties of the solid region are given in table 3. Here the properties of the solid are assumed to be constant and independent of temperature.

NUMERICAL METHOD.

The CFD code employed here is Ansys CFX 14.5. It uses an implicit finite volume formulation to construct the discretized equations representing the Reynolds Averaged Navier-Stokes equations for the fluid flow. The model consists of a compressible solver with a co-located (non-staggered) finite volume method, such that the control volumes are identical for

all transport equations [8]. The basic set of balance equations solved by ANSYS CFX comprises the continuity, momentum, species and energy transport equations. The instantaneous balance equations for the fluid domain in their conservative form can be written as :

continuity equation:

$$\frac{\partial \rho}{\partial t} + \nabla.(\rho U) = 0 \quad (1)$$

momentum equations:

$$\frac{\partial(\rho U)}{\partial t} + \nabla.(\rho UU) = -\nabla p + \nabla.\tau + s_m \quad (2)$$

where s_m represents the external momentum sources which can be due to buoyancy effects. However this term is neglected in these simulations. The stress tensor τ, is related to the strain rate by

$$\tau = \mu(\nabla U + (\nabla U)^T - \frac{2}{3}\delta \nabla.U) \quad (3)$$

Species:

$$\frac{\partial(\rho Y_i)}{\partial t} + \nabla.(\rho U Y_i) = -\nabla.J_i + R_i + S_i \quad (4)$$

where R_i is the net rate of production of species i by chemical reaction and S_i is the rate of creation by addition from the dispersed phase plus any user-defined sources.

total energy equation:

$$\frac{\partial(\rho h_{tot})}{\partial t} - \frac{\partial p}{\partial t} + \nabla.(\rho U h_{tot}) = \nabla.(\lambda_f \nabla T) + \nabla.(u.\tau) + u.s_m + s_e \quad (5)$$

where h_{tot} is the total enthalpy, related to the static enthalpy h (T, p) by:

$$h_{tot} = h + \frac{1}{2}U^2 \quad (6)$$

The term $\nabla.(u.\tau)$ represents the work due to viscous stresses and is called the viscous work term.

The term $u.s_m$ represents the work due to external momentum sources which is neglected in this work.

The source term s_e consists of the chemical and the radiative source terms, it also consists of the interphase energy source including the heat transfer between fluid and solid.

For the solid domain the equations solved are:

The energy equation for the solid is a simplified form of the energy equation for the fluid, which can account for heat transport due to solid motion, conduction and volumetric heat sources :

$$\frac{\partial(\rho_s h_s)}{\partial t} + \nabla.(\rho_s U_s h_s) = \nabla.(\lambda_s \nabla T) + s_e \quad (7)$$

where h_s, ρ_s and λ_s are the enthalpy, density, and thermal conductivity of the solid, respectively. Heat generation and dissipation is specified using the same s_e as for the fluid meaning that it can be due to chemical reaction, radiation or due to the heat transfer between different phases. However, In the current study, the source term in the equation 7 is just due to interphase energy which is coming from convective heat transfer between the solid and adjacent flow. The term including solid velocity of U_S takes into account the motion of the solid with respect to the reference frame. However it has been assumed here that the solid is stationary and no vibration or solid displacement will occur.

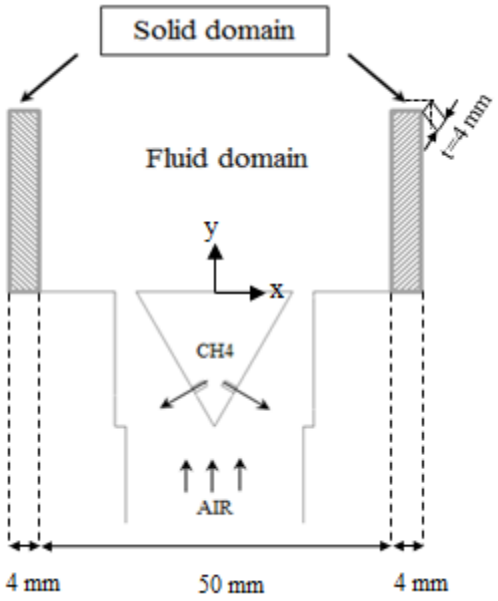

FIGURE 3: SKETCH OF THE FLUID AND SOLID REGIONS AS ONE COMPUTATIONAL DOMAIN

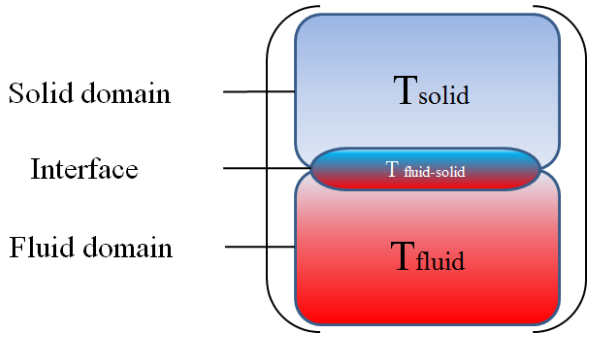

FIGURE 4: COUPLING THE FLUID AND STRUCTURE USING A MONOLITHICAL APPROACH

TABLE 1: PROPERTIES OF GRID FOR THE FLUID REGION

	Nodes	Elements
M_f	695976	644050

TABLE 2: PROPERTIES OF THREE MESHES USED FOR THE SOLID REGION

	M1	M2	M3
Nodes	7452	13550	27642
Elements	3304	8640	17280
First cell height [m]	2e-03	1e-03	1e-06

TABLE 3: SOLID (STAINLESS STEEL) CHARACTERISTICS OF THE TEST RIG

	Initial Temperature (K)	Thermal Conductivity ($\frac{W}{m.K}$)	Heat capacity ($\frac{J}{Kg.K}$)	Density ($\frac{Kg}{m^3}$))
Solid	300	60	434	7854

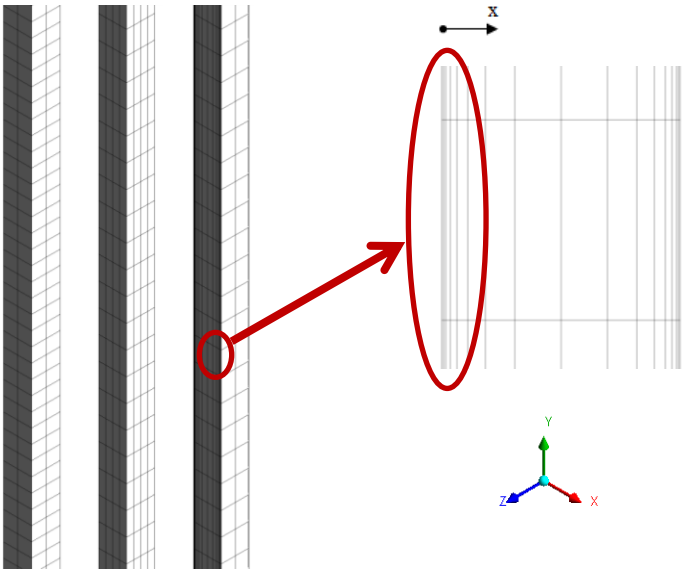

(a) (b) (c)

FIGURE 5:CLOSE UP VIEW OF THE SOLID DOMAIN (LEFT LINER) FOR THREE DIFFERENT GRID RESOLUTIONS : (A) M1, (B) M2 AND (C) M3

CFX solves equations for the RANS mean of the equations 1,2,5 in addition with equations for turbulence. Equation 4 is replaced by a transport equation for a reaction progress variable for combustion processes. In this paper, for the application to the conjugate heat transfer problem, the energy equations for the fluid and solid are solved simultaneously and the continuity of the energy flux is enforced at the fluid-solid interfaces, while all other transport equations are solved only for the fluid domain.

To avoid the decoupling of the pressure field, CFX uses the Rhie-Chow [9] discretization method for the mass terms, as modified by Majumdar [10]. A coupled algebraic multi-grid solver is used to give robust solutions for the governing system of linearized equations representing the differential transport equations in discretized form. For the discretization of the governing equations a high resolution advection scheme spatial method and a second order backward Euler discretization for time accuracy is used to solve the unsteady RANS- equations. In this work the effects of turbulence are simulated by using the Shear Stress Transport Turbulence Model (SST) in the steady state calculations, while for the transient calculations the Scale-Adaptive Simulation model (SAS) is used. The choice of turbulence model greatly influences the prediction of turbulent mixing rate and hence limit cycle oscillations. Comparison between the standard k-omega and SAS-SST model for the similar combustor has been reported earlier (see Santosh et al [11]).

Reacting flow simulations are carried out on the model combustor by using the Burning Velocity Model BVM using a new model option for improving accuracy for non-premixed flames [7, 12]. This model is coupled with the laminar flamelet PDF model to model post-flame front mixing and reaction. This mechanism involves 16 species and 46 reactions for methane-air gas mixture.

BOUNDARY CONDITION

Definition of the boundary condition is performed on basis of the known properties and behavior of the laboratory combustor. The CFD domain at the outlet end of the combustor has some additional length to represent the complex boundary condition in the form of an end correction. Therefore in the exhaust of the combustor, a zero relative pressure could be imposed. The mass flow rate of fuel and the velocity of the injected air are defined corresponding to table 4. Except for the interface surfaces, all solid boundaries are specified as wall with assigned no-slip condition, in which no mass and momentum are allowed in the direction perpendicular to them. The continuity of the energy flux is enforced at the fluid-solid interfaces. Since the outer surface of the solid parts is exposed to the ambient air and it is cooled by means of natural convection, the heat transfer coefficient and the external temperature are defined there.

All boundaries are set to be stationary in space and time, so the vibration of the liner is neglected. therefore the second term in the left hand side of equation 7 vanishes.

TABLE 4: OPERATING CONDITION

Power (kW)	Air factor	Methane mass flow rate [g/s]	Air mass flow rate [g/s]
40	1.4	0.8	19.152

RESULTS AND DISCUSSIONS.

GRID EFFECT IN THE SOLID REGION

This section presents results obtained for a CHT approach using different grid sizes in the solid region, and compares them to the experimental data. The combustor presents self-exited oscillations of high amplitude which are linked to the phase relationship between the acoustic pressure field and unsteady heat release. The measured frequencies of the instability are more related to the acoustic eigen modes of the combustion chamber [7]. Experimental results from the gas pressure measurements are obtained from the installed pressure transducers which are shown in figure 2 for a location 200 mm above the burner. This data was seen as a good validation tool

for the investigation of the conjugated heat transfer calculation and the sensitivity of results to the used grid for the solid region. Since the solid has been modelled explicitly then it is required to start the transient simulation from a steady state calculation in which the solid temperature has reached equilibrium with the hot combustion gases and the outside temperature. In the transient simulation the same time step for fluid and solid domain has been set, with a maximum value dictated by the acoustic CFL number. The residuals are small enough at the end of each time step to resolve the small changes in temperature at the surface of the solid. The convergence of residuals for all variables except for energy were resolved to a level of 1e-5. For the energy equation it is in the order of 1e-7.

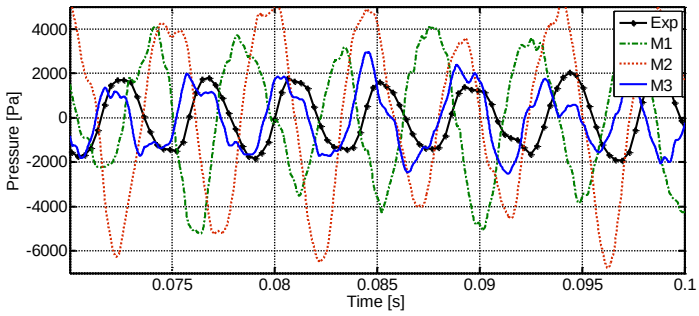

FIGURE 6: MEASURED AND PREDICTED PRESSURE SIGNAL

Figure 6 shows how the grid size in the solid region changes the results of the simulation. Although it seems that the predicted value by the mesh (M1) is not as far from the experiment as of the grid (M2) is, running the simulation for longer period of time shows that there is just a bigger time delay in this case to reach a saturated limit cycle oscillation at a higher pressure level than the predicted value by the grid (M2), meaning that after certain time the pressure level in this case also reaches to 6000 Pa. This might be due to the large thermal inertia of the wall which requires much greater timescales to find the equilibrium state than required for the fluid flow. It can be concluded that the amplitude of pressure oscillations is highly dependent on the grid size, and can be over predicted by a factor of 2 or even 3 (in the case that the first layer of grid in the solid is as far as 1 mm away from the fluid-solid interface).

Here, the knowledge and analytical solutions for transient solid thermal behavior can be used for interpretation, as available from the semi-infinite solid approach. This can be used to determine and interpret the transient response of the solid. Because the solid region in this simulation is a finite body, the approximation would be valid for the behavior of the transient, neglecting the mean temperature gradient and effect of the proximity of the outer surface. For instance for the time scale of dt=1e-5 s, heat can penetrate into the solid only a distance of $dx \propto \sqrt{\alpha dt}$, where α is the thermal diffusivity, $\alpha = k/(\rho c_p)$. For the current parameter settings this gives the penetration depth in order of magnitude of microns! Then by creating coarser grids, the heat penetration depth will be discarded by the calculation and the surface temperature of the solid will not be predicted to change on short time scales and the heat transfer to (and from) the solid will be either over or under estimated, resulting in a low/high magnitude of the pressure fluctuations. More details are given in Annex A. Therefore by adding an inflation layer on the solid side of the fluid-solid interface with a first cell height of 1e-6 m the resolution is increased, giving closer prediction to the experimental measurements. That explains why the predicted results by grid (M3) is more accurate and close to the experiments.

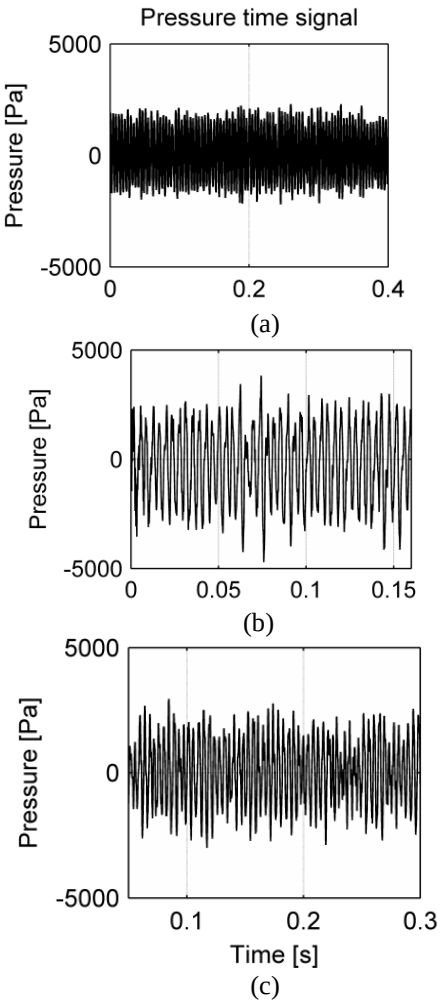

FIGURE 7: PRESSURE SIGNAL CAPTURED AT Y= 200 MM FROM (A) EXPERIMENT (B) FLUID-ONLY CALCULATION WITH ISOTHERMAL LINER (C) CHT APPROACH (THE USED GRID IS M3)

The pressure signal obtained from the CHT calculation and also from the fluid-only simulation with the isothermal liner as well as the measured data are presented in figure 7. In the isothermal case the temperature of the liner is assumed to be kept at 1000 K. The simulation with isothermal liner settings over-predicts the amplitude of the pressure oscillations, while the CHT

approach gives a much better prediction. This can be clearly observed in figure 8.

The first peak frequency observed, which is associated with the first harmonic of the downstream part of the combustor [13] is presented in table 5 for both CFD and experiments. According to this table, the first excited mode of the considered case is well predicted by the CHT model, and the error in the CFD calculation is 0.6 %. While in the case of fluid-only simulation, assuming constant liner temperature, results in about 10% error. Apparently the amount of heat, transferred from the hot gases to the liner and then surrounding, is under-predicted in the fluid-only calculation, resulting in higher speed of sound and hence higher frequency of instability. Since the prediction of the unstable frequency of the combustor is of great importance CHT modeling is recommended for highest accuracy.

Figure 9 represents the pressure spectrum post processed of the time signal. As it can be seen the periodic oscillation of the pressure signal in the time domain appears as a peak frequency of about 232 Hz surrounded by many secondary peaks, the source of these peaks is discussed in [7, 14]. The mode at about 600 Hz which is missing in the CFD prediction, corresponds to the structural mode of the combustor. Overall good comparison between the measured data and the CHT results is achieved.

HEAT TRANSFER

Heat flux at the wall of the combustor represents the transfer of energy from the operating gas to the solid walls in contact. Capturing the near-wall behavior of the hot gases in contact with the solid is a step towards better understanding of the heat transfer process.

In the previous section the effect of the grid size, especially the first cell height, on the accuracy of the results was discussed. Therefore all the results from now on correspond to the most accurate grid (M3). Figure 10 shows the transient time averaged temperature field in the both solid and fluid regions. The simulation has been done for the total physical time of 0.3 second, hence data is averaged over approximately 75 cycles. It should be noticed that the temperature contour presented here corresponds to just 200 mm of the full height of the combustion chamber. According to figure 10 burnet gases reach to a temperature of 2000 K, while the wall temperature remains between 500 and 900 K. Therefore the temperature should decrease from the hot gases level to the wall level; this change occurs in a near-wall layer and creates large temperature gradients. That is the reason for using a high density of very small grid cells in the near wall region in both domains of interest. The achieved solution is far from the assumed isothermal wall at 1000 K or other calculations done for the same combustor imposing the adiabatic boundary condition on the wall [15]. The underestimations of the convective heat transfer in the first case leads to under prediction of the heat flux at the liner. This can be observed in figure 11 along the line of Z=0 over the Y-Z plane. The heat loss through the wall predicted by the CHT approach is more than that of predicted by the fluid-only calculations with the isothermal liner. The difference in the predicted heat loss by these two mentioned approaches is significant especially within the 200 mm distance from the wedge, while above that height using the CHT approach does not change the prediction much. The modelling of the heat transfer in this first 200 mm height of the liner, where the main combustion reactions occur, is very critical to estimate the correct frequency and amplitude of instabilities.

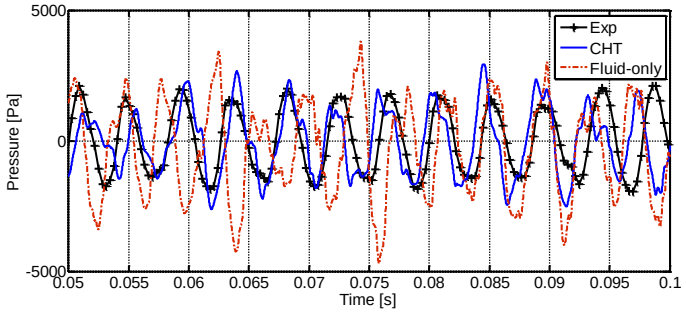

FIGURE 8: PRESSURE EVOLUTION OVER 0.05 SECOND CALCULATED WITH DIFFERENT APPROACHES

TABLE 5: CALCULATED AND MEASURED THE FIRST SELF-EXCITED MODES

	CFD		Experiment
	Isothermal liner	CHT	
f_1 (Hz)	256	232	234

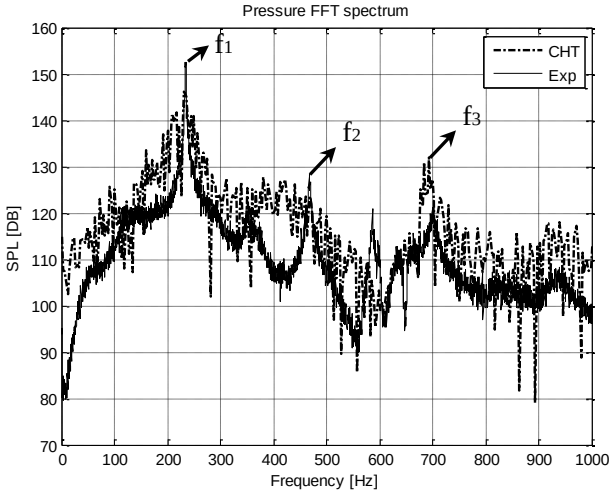

FIGURE 9: PRESSURE SPECTRUM FOR 40KW AND Λ=1.4 : EXPERIMENT (SOLID LINE), CHT (DASH-DOT)

The time averaged transient solution of the wall adjacent gas temperature, which is defined as the average temperature of hot gases in the control volume next to the wall is shown in figure 12 for the different approaches. The maximum achieved temperature in the CHT model and fluid-only model with the

isothermal liner occurs in the location of the maximum heat flux (as presented in figure 11), where the maximum heat transfer from the hot gases to the colder liner is taking place. While in the case with adiabatic liner after 100 mm above the flame holder the temperature reaches 2030 K and it remains constant which is very far from what predicted by other approaches.

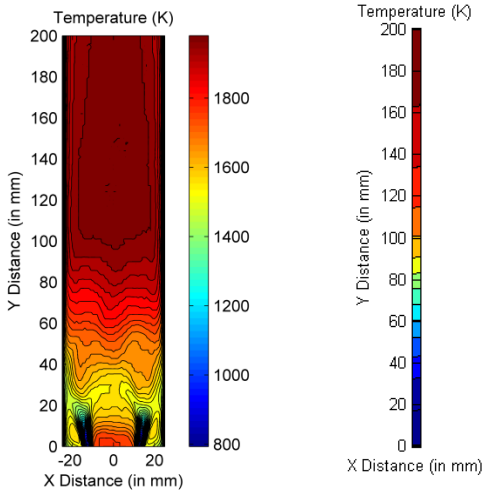

(a) (b)

FIGURE 10: TRANSIENT TIME AVERAGED TEMPERATURE IN THE PLANE Z=0 FOR (A) FLUID DOMAIN, (B) SOLID DOMAIN

Figure 13 shows the predicted heat transfer coefficient (hc) over the interface surface. The observation is that in the first 50 mm of the liner the heat transfer coefficient is increasing and then afterwards it starts to decrease; however it increases again after y=100 mm and reaches the maximum value of 98 $\left(\frac{W}{m^2.K}\right)$ between 150 and 250 mm; while going further downstream it remains almost constant. It is worthwhile to pay more attention to the wall heat flux plotted in figure 11. This plot shows that the maximum heat loss occurs at the location of y=71 mm which is not the place of maximum h . This may be ascribed to the higher temperature gradient, which renders heat transfer on this location higher (see figure 12
figure 12), as the wall heat transfer coefficient, h_c is defined based on T_{wall} and the wall adjacent temperature,
Contour plots from CHT and fluid-only simulations showing the temperature distribution over time are given in figure 14. The temperature evolution in the CHT case takes longer time meaning that the acoustic limit cycle oscillation has a lower frequency/longer period. The incoming mixture of air and the fuel travels further beyond the flame holder before it is getting ignited, and still after 100 mm above the wedge, some cold spots of fresh mixture penetrating to the hot products can be observed cooling down the hot gases. This leads to a lengthening of the reattachment region and makes the central recirculation zone more stretched. Earlier it was already observed that assuming the isothermal liner predicts oscillations with shorter wavelength and therefore higher frequency. In this case, there is no remaining fuel far downstream, everything is consumed before 50 mm. As it is expected due to modeling the heat loss through and within the liner, the temperature in the CHT case is generally lower than in the isothermal liner case.

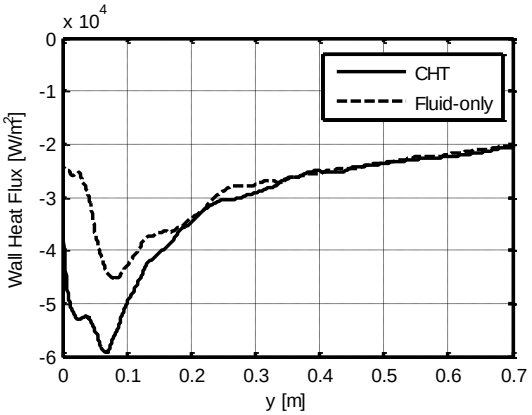

FIGURE 11: PREDICTED HEAT FLUX THROUGH THE INNER SURFACE OF THE LINER (OVER Z-Y PLANE, ALONG THE LINE OF Z=0) WITH DIFFERENT APPROACHES

CONCLUSION AND FUTURE WORK

Transient fluid-structure thermal analyses of the Limousine combustor have been conducted for better prediction of unstable modes of the combustor as well as estimating the temperature distribution of the liner during the LCO. In this approach a simultaneous solution procedure has been used, meaning that the coupled equations for both solid and fluid domain are solved together. The calculation has been done by using the CFX code and defining the same time scales for both fluid and solid regions. This time step is indeed the smallest time scale of the problem. Therefore the coupling between the structure and the fluid is very strong at the interface. Pressure data has been used as a validation tool. Due to the existence of high temperature in the chamber and also temperature fluctuation during the limit cycle oscillation, it is very difficult to measure the temperature with the thermocouples. That is why the temperature data is not presented here. The pressure oscillations are not only regulated by the heat transfer, however since all parameters which may affect the pressure fluctuations are kept constant, the imposed thermal boundary condition remains the only varying parameter affecting the pressure oscillations and therefore acoustic. Considering the previous calculations concerning the effects of turbulence and combustion modeling [7,11], the improvement on the prediction of the pressure oscillations is just dependent on the thermal behavior of the system. For this reason pressure data can be used as a verification tool. The present study has revealed the following observations:

- Although it seems that the solid grid size is less stringent and does not have much influence on the accuracy of the results, current calculations show that the evaluation of the pressure oscillation amplitude highly depends on the height

of the first layer of the grid close to the solid interface, which should be in order of sqrt(αdt).

- CHT prediction results are in very good accordance with the pressure measurements. The results demonstrate that application of transition CHT model in calculations can more accurately predict the unstable mode of the combustor (just 0.6% error) which is very promising and showing the ability of current schemes to predict the instability of combustion systems. The obtained result also proves that URANS simulations can render such a complex flow reliably.
- It was shown that the heat flux obtained by fluid-only simulation and by the CHT are very much different within a distance of 0-200 mm above the flame holder, while they are very similar all along the remaining distance up to the exhaust plane.

In this current study, the dependence of the input parameters on the temperature distribution has not been taken to account. However it is worth checking the uncertainty of the material properties (for instance the thermal conductivity), and deserves further investigation.

ACKNOWLEDGMENTS

The authors would like to acknowledge the funding of this research by the EC in the Marie Curie Actions Networks for Initial Training, under call FP7-PEOPLE-2007-1-1-ITN, Project LIMOUSINE with project number 214905. Special thanks go to Dr. Phil Stopford for the support in the use of ANSYS-CFX.

REFERENCES

[1] Boudier, G., Gicquel, L. Y. M., Poinsot, T., Bissières, D., and Bérat, C., 2007, "Comparison of LES, RANS and experiments in an aeronautical gas turbine combustion chamber," Proceedings of the Combustion Institute, 31(2), pp. 3075-3082.

[2] Duchaine, F., Corpron, A., Pons, L., Moureau, V., Nicoud, F., and Poinsot, T., 2009, "Development and assessment of a coupled strategy for conjugate heat transfer with Large Eddy Simulation: Application to a cooled turbine blade," International Journal of Heat and Fluid Flow, 30(6), pp. 1129-1141.

[3] Duchaine, F., Mendez, S., Nicoud, F., Corpron, A., Moureau, V., and Poinsot, T., 2009, "Conjugate heat transfer with Large Eddy Simulation for gas turbine components," Comptes Rendus Mécanique, 337(6–7), pp. 550-561.

[4] Duchaine, F., Maheau, N., Moureau, V., Balarac, G., and Moreau, S., "Large Eddy Simulation and Conjugate Heat Transfer Around a Low-Mach Turbine Blade," Proc. In proceeding of: ASME Turbo Expo 2013, GT2013-94257.

[5] Mazur, Z., Hernández-Rossette, A., García-Illescas, R., and Luna-Ramírez, A., 2006, "Analysis of conjugate heat transfer of a gas turbine first stage nozzle," Applied Thermal Engineering, 26(16), pp. 1796-1806.

[6] Shahi, M., Kok, J. B. W., Sponfeldner, T., and Pozarlik, A., 2013, "Thermal and fluid dynamic analysis of partially premixed turbulent combustion driven by thermo acoustic effects," ICSV20,Bangkok, Thailand.

[7] Shahi, M., Kok, J. B. W., Pozarlik, A. K., Roman Casado, J. C., and Sponfeldner, T., "Sensitivity of the numerical prediction of flow in the limousine combustor on the chosen mesh and turbulent combustion model," Proc. Proceedings ASME Turbo Expo 2013, GT2013-94328.

[8] Patankar, S. V., 1980, Numerical Heat Transfer and Fluid Flow, Hemisphere Publishing Corp.

[9] C.M.Rhie, and W.L.Chow, 1982, "a numerical study of Turbulent Flow Past an Isolated Airfoil with the Trailing Edge Separation," Aiaa Journal, pp. 82-0998.

[10] Majumdar, S., 1988, "Role of underrelaxation in momentum interpolation for calculation of flow with

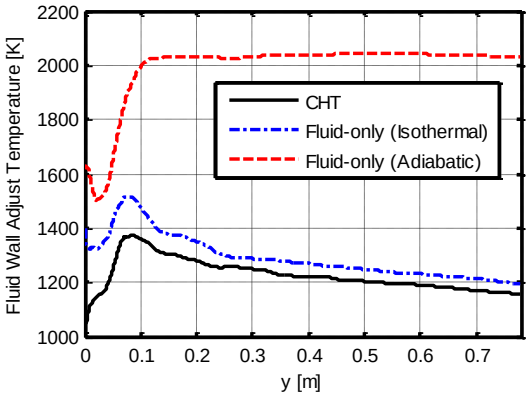

FIGURE 12: WALL ADJACENT TEMPERATURE ALONG THE HEIGHT OF THE COMBUSTOR

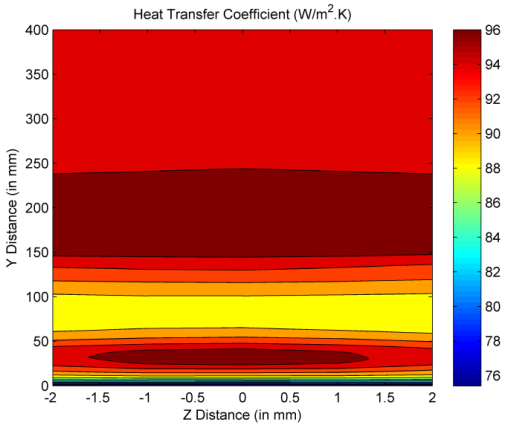

FIGURE 13: WALL HEAT TRANSFER COEFFICIENT PREDICTED USING CHT MODEL

nonstaggered grids," Numerical Heat Transfer, 13(1), pp. 125-132.
[11] Santosh Kumar, T. V., Alemela, P. R., and Kok, J. B. W., "Dynamics of flame stabilized by triangular bluff body in partially premixed methane-air combustion," Proc. ASME Turbo-Expo 2011, GT2011-46241.
[12] Forkel, H., 2012, ANSYS manual, "Modification to the burning velocity model at ANSYS Germany."
[13] Roman Casado, J. C., and Kok, J. B. W., "Non-linear effects in a lean partially premixed combustor during limit cycle operation," Proc. Proceeding of ASME Turbo Expo 2012, GT2012-69164.
[14] Roman Casado, J. C., 2013, "Nonlinear behavior of the thermoacoustic instabilities in the limousine combustor," PhD, University of Twente, Enschede.
[15] Hernández, I., Staffelbach, G., Poinsot, T., Román Casado, J. C., and Kok, J. B. W., 2013, "LES and acoustic analysis of thermo-acoustic instabilities in a partially premixed model combustor," Comptes Rendus Mécanique, 341(1–2), pp. 121-130.
[16] Incropera, F. P., and DeWitt, D. P., 2002, Fundamentals of heat and mass transfer, John Wiley & Sons Australia, Limited.

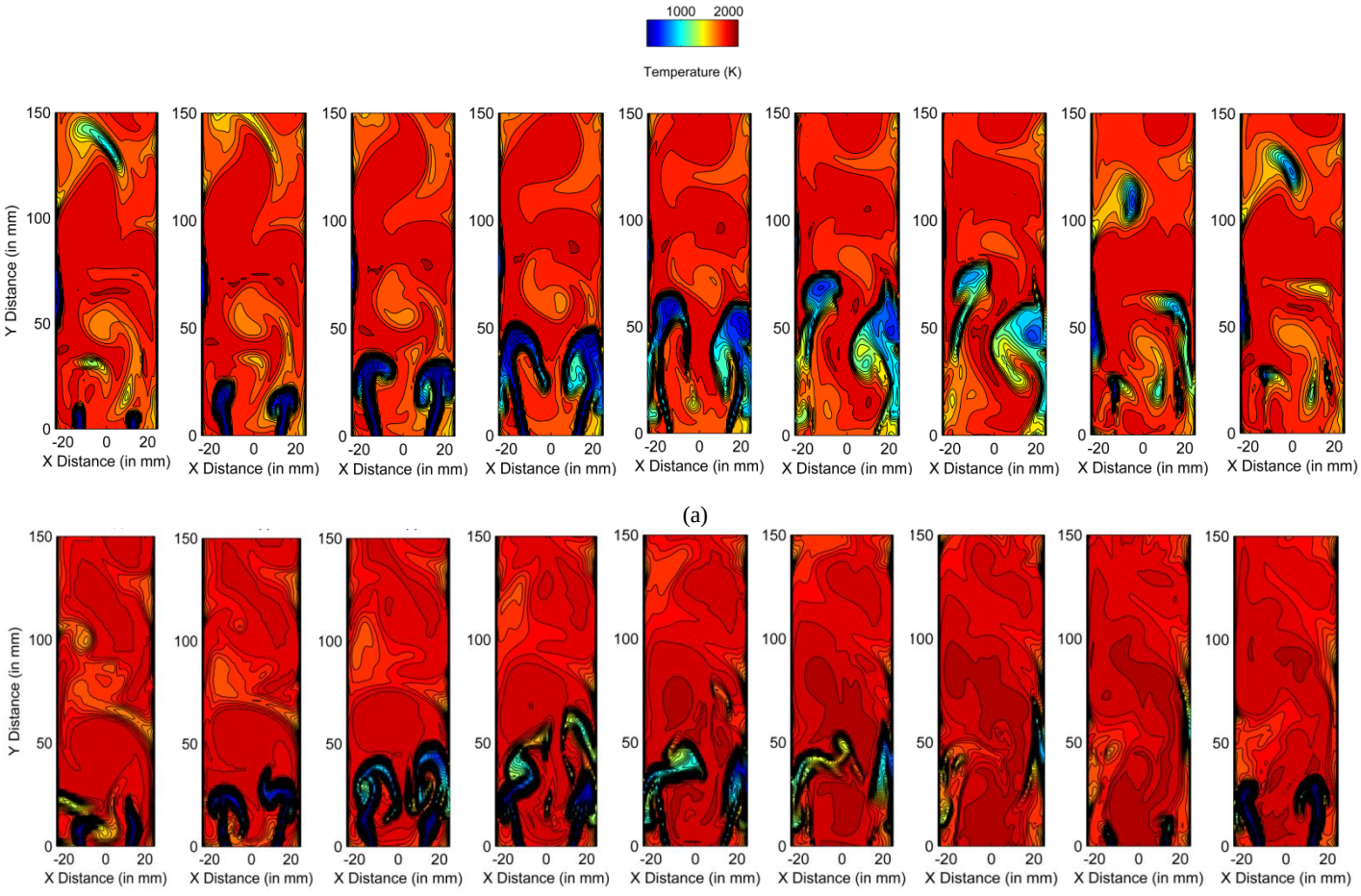

FIGURE 14: INSTANTANEOUS GAS TEMPERATURE CONTOURS (OVER ONE CYCLE OF OSCILLATION) FOR THE (A) COMBUSTOR INCLUDING THE SOLID (CHT) (B) FLUID-ONLY SIMULATION WITH THE ISOTHERMAL LINER (IN THIS FIGURE THE SAME TEMPERATURE SCALE IS USED FOR ALL CONTOURS

ANNEX A
ONE-DIMENSIONAL TRANSIENT HEAT CONDUCTION IN SEMI-INFINITE BODY

A semi-infinite solid is an idealized body that has a single plane surface and extends to infinity in all directions. For short periods of time, most bodies can be modeled as semi-infinite solids since heat does not have sufficient time to penetrate deep into the body, and the thickness of the body does not enter into the heat transfer analysis.

The heat equation for transient conduction in a semi-infinite solid is given by :

$$\frac{\partial T}{\partial x^2} = \frac{1}{\alpha}\frac{\partial T}{\partial t} \qquad 8$$

To solve this equation, an initial condition and two boundary conditions should be specified, which in this case can be expressed as:

$$T(x,0) = T_i \quad (9)$$

$$T(0,t) = T_s \quad (10)$$

$$T\left(x \to \infty, t\right) = T_i \quad (11)$$

The temperature near the surface of the semi-infinite body will increase because of the surface temperature change, while the temperature far from the surface of the semi-infinite body is not affected and remains at the initial temperature T_i. (see figure 15)

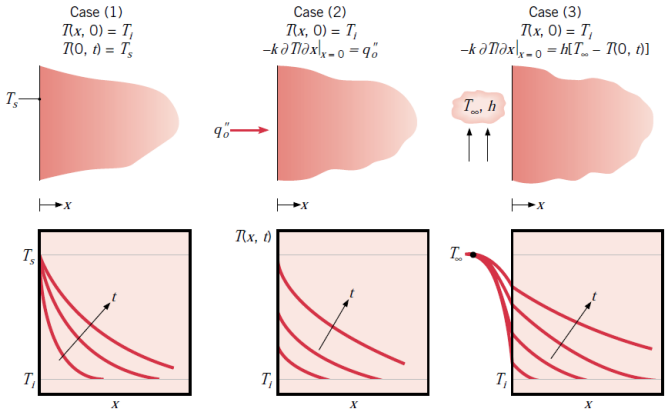

FIGURE 15: TRANSIENT TEMPERATURE DISTRIBUTIONS IN A SEMI-INFINITE BODY FOR THREE DIFFERENT BOUNDARY CONDITIONS (THIS FIGURE IS TAKEN FROM REFERENCE [16])

The analytical solution of the problem can be found in [16]. The temperature distribution and the heat transfer can be expressed as :

$$\frac{T(x,t) - T_s}{T_i - T_s} = \operatorname{erf}\left(\frac{x}{2\sqrt{\alpha t}}\right) \quad (12)$$

$$q_s''(t) = \frac{k(T_s - T_i)}{\sqrt{\alpha t}} \quad (13)$$

Where erf(w) is the Gaussian error function and is defined as :

$$\operatorname{erf(w)} = \frac{2}{\sqrt{\pi}} \int_0^w e^{-v^2} dv \quad (14)$$

According to the definition of the thermal penetration depth, the temperature, at the thermal penetration depth should satisfy the following conditions:

$$\frac{\partial T(x,t)}{\partial x} = 0 \quad at \quad x = \delta(t) \quad (15)$$

$$T(x,t) = T_i \quad at \quad x = \delta(t) \quad (16)$$

By integrating equation 15 in the interval $(0, \delta)$, it can be written as :

$$\left.\frac{\partial T}{\partial x}\right]_{x=\delta(t)} - \left.\frac{\partial T}{\partial x}\right]_{x=0} = \frac{1}{\alpha}\int_0^{\delta(t)} \frac{\partial T(x,t)}{\partial t} dx \quad (17)$$

The right hand side of equation 17 can be rewritten as :

$$\left.\frac{\partial T}{\partial x}\right]_{x=\delta(t)} - \left.\frac{\partial T}{\partial x}\right]_{x=0} = \frac{1}{\alpha}\left[\frac{d}{dt}\left(\int_0^{\delta} T\, dx\right) - T\right]_{x=\delta}\frac{d\delta}{dt}\Bigg] \quad (18)$$

which represents the energy balance within the thermal penetration depth. Substituting equations 15 and 16 into equation 18 yields:

$$-\alpha \left.\frac{\partial T}{\partial x}\right]_{x=0} = \frac{d}{dt}(\theta - T_i\delta) \quad (19)$$

Where

$$\theta(t) = \int_0^{\delta(t)} T(x,t)\, dx \quad (20)$$

By assuming that the temperature distribution in the thermal penetration depth is a third-order polynomial function of x , and considering that The surface temperature of the semi-infinite body, T_s is not a function of time, the temperature distribution in the thermal penetration depth becomes :

$$\frac{T(x,t) - T_i}{T_s - T_i} = 1 - \frac{3}{2}\left(\frac{x}{\delta}\right) + \frac{1}{2}\left(\frac{x}{\delta}\right)^3 \quad (21)$$

where the thermal penetration depth, δ, is still unknown. Substituting equation 21 into equation 19, an ordinary differential equation for δ is obtained:

$$4\alpha = \delta\frac{d\delta}{dt} \qquad t > 0 \quad (22)$$

Since the thermal penetration depth equals zero at the beginning of the heat conduction, the thermal penetration depth for a semi-infinite body can be written as:

$$\delta = \sqrt{8\alpha t} \quad (23)$$

The surface may also exposed to a constant heat flux $q_0^{"}$ or to a fluid characterized by $T_\infty$and the convection coefficient of h. The temperature distribution in the first case can be expressed as :

$$T(x,t) - T_i = \frac{2q_0^{"}\sqrt{\alpha t/\pi}}{k}\exp\left(\frac{-x^2}{4\alpha t}\right) - \frac{q_0^{"}x}{k} erfc\left(\frac{x}{2\sqrt{\alpha t}}\right) \quad (24)$$

While in the second case when the surface is expose to the convection heat transfer, the temperature distribution can be written as :

$$\frac{T(x,t) - T_s}{T_i - T_s} = \operatorname{erf}\left(\frac{x}{2\sqrt{\alpha t}}\right) - \left[\exp\left(\frac{hx}{k} + \frac{h^2\alpha t}{k^2}\right)\right]\left[erfc\left(\frac{x}{2\sqrt{\alpha t}} + \frac{h\sqrt{\alpha t}}{k}\right)\right] \quad (25)$$

The complementary error function $erfc(w)$is defined as $(1 - \operatorname{erf(w)})$.